



OPEN

Impact toughness and dynamic constitutive model of geopolymer concrete after water saturation

Tiecheng Yan¹, Xiangxiang Yin^{2,3}✉ & Xingyuan Zhang¹

The dynamic compression test of geopolymer concrete (GC) before and after water saturation was carried out by the split Hopkinson pressure bar (SHPB). And the effects of water saturation and strain rate on impact toughness of GC were studied. Based on Weibull statistical damage distribution theory, the dynamic constitutive model of GC after water saturation was constructed. The results show that the dynamic peak strain and specific energy absorption of GC have strain rate strengthening effect before or after water saturation. The impact toughness of GC decreases after water saturation. The size distribution of GC fragments has fractal characteristics, and the fractal dimension of GC fragments after water saturation is smaller than that before water saturation. The dynamic constitutive model based on Weibull statistical damage distribution theory can accurately describe the impact mechanical behavior of GC after water saturation, and the model fitting curves are in good agreement with the experimental stress–strain curves.

Keywords Geopolymer concrete, Water saturation, Impact toughness, Constitutive model, Statistical damage distribution theory

Geopolymer concrete (GC) is a new building material. Because of its low energy consumption, low carbon dioxide emissions, and large consumption of industrial solid waste in the production process, GC is reputed as the “green and environment-friendly material” in the twenty-first century^{1–3}. Researches have shown that GC not only has high strength and good workability, but also has excellent durability, which makes GC can be used in hydraulic engineering and has a wide application prospects in hydraulic structures (such as dams, locks, docks and bridges)^{4–6}.

There are many tiny pores inside the concrete. When serving in the water environment, its internal pores are saturated or semi-saturated, which will affect the mechanical properties of concrete. Many researches have shown that the mechanical properties of concrete after water saturation are quite different from those at the dry state^{7,8}. At present, the researches on the mechanical properties of concrete after water saturation are mainly limited to quasi-static cases, and there are still some deficiencies among the researches of its dynamic mechanical properties^{9–11}. Rossi et al. studied the effect of free water on the properties of concrete under tensile stress, and explained the change mechanism of mechanical properties of concrete after water saturation. But they did not study the compressive strength of concrete^{12,13}. Mehta et al. and Vu et al. studied the strength characteristics of concrete under various moisture content states, but did not deeply explore the mechanism of free water^{14,15}. Zhang et al. compared the change law of compressive strength of concrete after water saturation under different loading rates, but the loading rates were less than 10^{-4} s^{-1} , which still belonged to the quasi-static loading state¹⁶.

As a rate-sensitive material, concrete will show different mechanical properties under impact load and static load^{17–20}. And in the actual service environment, hydraulic concrete structures are inevitably subjected to dynamic loads such as ship strikes, underwater blasting, seismism and so on^{21–24}. Therefore, it is of great significance to study the dynamic mechanical properties of concrete after water saturation for underwater blasting excavation, underwater building demolition and seismic safety assessment of large underwater buildings. Based on this, the dynamic compression test of GC after 180 d immersing in-water was carried out by the $\Phi 100$ mm split Hopkinson pressure bar (SHPB). And the impact toughness and fracture morphology of GC before and after water saturation were compared and analyzed. Based on the Weibull statistical damage distribution theory, the dynamic constitutive model of GC after water saturation was constructed.

¹College of Civil Engineering, Longdong University, Qingyang 745000, China. ²Hydrochina Chengdu Engineering Corporation Limited, Chengdu 610072, China. ³College of Water Conservancy and Hydropower, Hohai University, Nanjing 210098, China. ✉email: yantiechengldxy@163.com

Experiment

Preparation of specimens

The raw materials of GC include cementitious materials, alkaline activators, gravel, sand and water. Cementitious materials include slag and fly ash. Alkali activators include NaOH and sodium silicate. The purity of NaOH is more than 97%. The modulus Sodium silicate ($\text{SiO}_2/\text{Na}_2\text{O}$) is 3.1 ~ 3.4, the SiO_2 content is more than 26.0%, and the Na_2O content is more than 8.2%. Gravel: limestone gravel with a density of 2.70 g/cm^3 , a particle size of 5 ~ 20 mm, and a mud content of 0.2%. Sand: medium sand with a fineness modulus of 2.8, a density of 2.63 g/cm^3 , and a mud content of 1.1%. Water: clean tap water.

GC was prepared according to the mix proportion shown in Table 1. (1) NaOH, sodium silicate and water were mixed and stirred evenly to prepare mixture solution. (2) Sand and half of the mixture solution were added to the concrete mixer and stirred for 30 s. (3) Gravel was added to the concrete mixer and stirred for 30 s. (4) Slag and fly ash were added to the concrete mixer and stirred for 60 s. (5) The remaining mixture solution was added to the concrete mixer and stirred for 120 s. (6) Molding, vibrating and curing. The size of specimen is $\Phi 100 \text{ mm} \times 50 \text{ mm}$, as shown in Fig. 1.

After standard curing of 28 d, the specimens were divided into two groups. One group of specimens (GC-D) continued standard curing for 180 d. And the other group of specimens (GC-W) were immersed in water for 180 d to make them saturated, and then they were taken out for testing.

Experimental method

The dynamic compression test of GC was carried out by the $\Phi 100 \text{ mm}$ SHPB (as shown in Fig. 2). The aluminum wafers were used as the waveform shaper in the test, as shown in Fig. 3. The strains of incident, reflected and transmitted waves were measured by strain gauge, and then the test data are processed by Eq. (1), so as to obtain the stress–strain curves²⁵.

Slag	Fly ash	NaOH	Sodium silicate	Gravel	Sand	Water
249	110	25	88	1016	810	88

Table 1. The mix proportion of GC (kg/m^3).

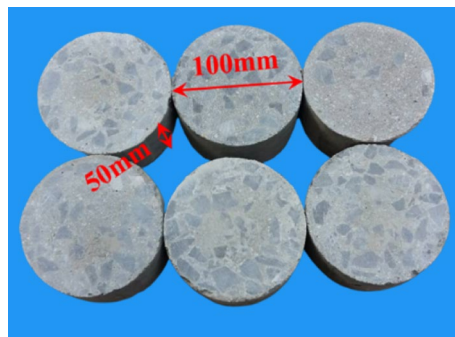


Figure 1. The GC specimen.

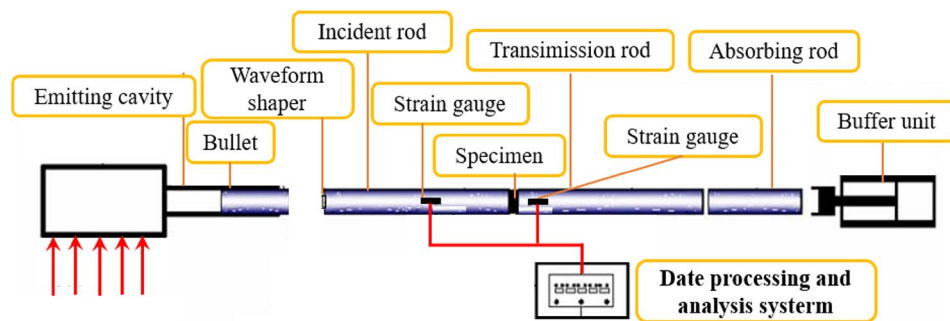


Figure 2. The $\Phi 100 \text{ mm}$ SHPB.

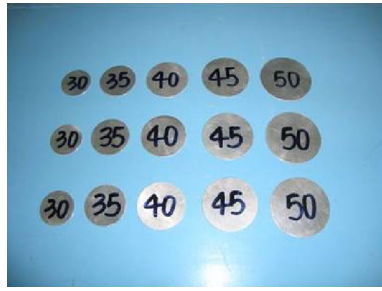


Figure 3. Aluminum wafers.

$$\begin{aligned}\sigma(t) &= \frac{E_e A_e}{2A_s} [\varepsilon_I(t) + \varepsilon_R(t) + \varepsilon_T(t)] \\ \varepsilon(t) &= \frac{C_e}{L} \int_0^t [\varepsilon_I(t) - \varepsilon_R(t) - \varepsilon_T(t)] dt \\ \varepsilon'(t) &= \frac{C_e}{L} [\varepsilon_I(t) - \varepsilon_R(t) - \varepsilon_T(t)]\end{aligned}\quad (1)$$

where σ , ε and ε' are the stress, strain and strain rate, respectively. ε_I , ε_R and ε_T are the strains of incident, reflected and transmitted waves, respectively. L is 50 mm. A_e and A_s are 7850 mm². E_e and C_e are 210 GPa and 5172 m/s, respectively.

The incident wave after shaping is shown in Fig. 4. From this figure, the incident wave before shaping is a trapezoidal wave, and the incident wave overshoot phenomenon is obvious. The total loading time (T) and time of rising segment (t) of incident wave are 288 μ s and 101 μ s, respectively. The incident wave after shaping is a half-sine wave, and the incident wave overshoot phenomenon is improved. The T of the incident wave increases to about 500 μ s, and the t increases to 175 μ s. The incident wave after shaping can ensure that the specimen has enough time to achieve stress uniformity before failure and achieve approximate constant strain rate loading.

The original waves and strain rate time-course curve after shaping are shown in Fig. 5 and Fig. 6, respectively. From Fig. 5, $\varepsilon_I + \varepsilon_R = \varepsilon_T$, indicating that the specimen reaches a uniform stress state. From Fig. 6, approximate constant strain rate loading was achieved during the test. The stress–strain curves obtained by the test are shown in Fig. 7.

Results and discussion

Impact toughness

Impact toughness is an important index to measure the dynamic mechanical properties of materials, which reflects the deformation and energy absorption capacities of materials²⁶. The indexes for evaluating the impact toughness of GC are dynamic peak strain and specific energy absorption. Dynamic peak strain reflects the deformation characteristics of GC. Specific energy absorption is the area formed by the stress–strain curve and coordinate axis, which reflects the energy absorption characteristics of GC.

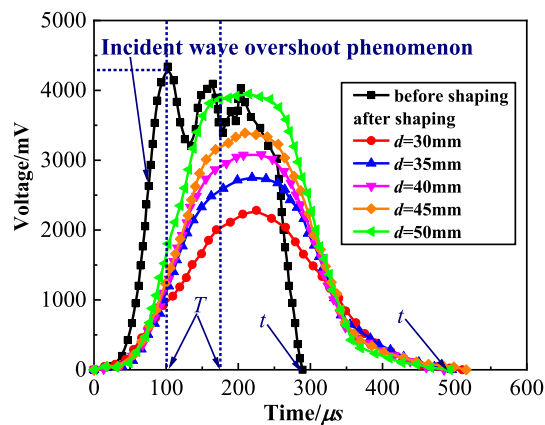


Fig. 4. The incident wave after shaping.

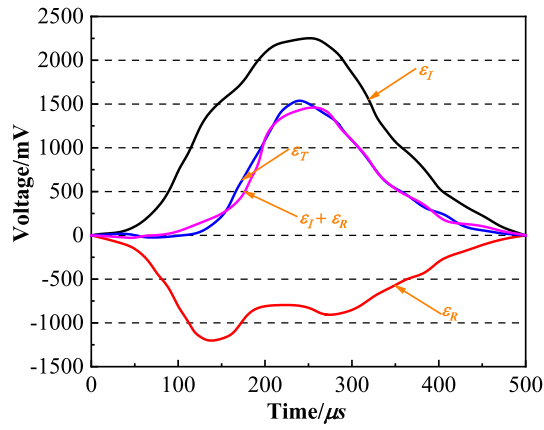


Figure 5. The original waves after shaping.

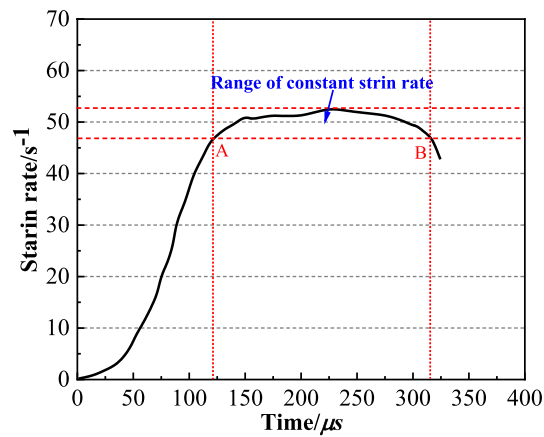
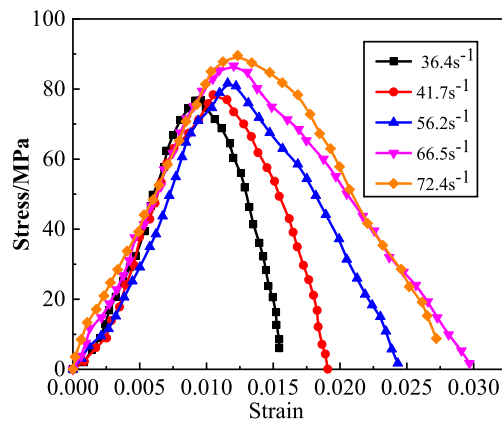
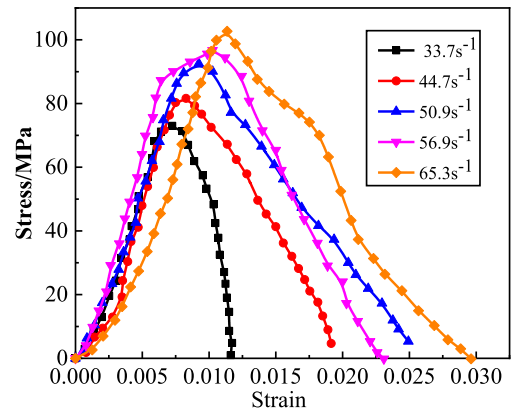


Figure 6. The strain rate time-course curve.



(a) GC-D



(b) GC-W

Figure 7. The stress–strain curves of GC.

Dynamic peak strain

The dynamic peak strain (ε) of GC is shown in Fig. 8. From this figure, the strain rate strengthening effect of the ε of GC before or after water saturation is significant. With the increase of strain rate, the ε increases linearly. At the same strain rate, the ε of GC before water saturation is larger than that after water saturation. In order to quantitatively analyze the influence of water saturation on the ε of GC, the change rate of dynamic peak strain ($\bar{\varepsilon}$) is defined, as shown in Eq. (2).

$$\bar{\varepsilon} = (\varepsilon_{GC-W} - \varepsilon_{GC-D}) / \varepsilon_{GC-D} \quad (2)$$

where ε_{GC-W} is the ε of GC after water saturation, ε_{GC-D} is the ε of GC before water saturation. The $\bar{\varepsilon}$ of GC is shown in Fig. 9. From this figure, the deformation characteristics of GC decreases after water saturation. With the increase of strain rate, the $\bar{\varepsilon}$ of GC after water saturation increases continuously. When the strain rate is small, the ε of GC after water saturation decreases significantly. When the strain rate is large, the extent of the decrease of the ε of GC after water saturation is small. The maximum extent of the decrease of the ε of GC after water saturation is 26.16%.

It can be seen from the test results that the deformation characteristics of GC decreases after water saturation. The main reason is that the free water in pores and cracks limits the deformation of GC, which reduces its dynamic peak strain. GC is a heterogeneous material, which contains different types and sizes of pores and cracks. On the one hand, water in the pores and cracks of GC is more difficult to compress than air. Under the impact load, the volume of water is difficult to change, and the water is difficult to discharge in a short time^{12,27}. Therefore, the water in the pores and cracks of GC after water saturation limits the deformation of it. On the other hand, according to the micro fluid mechanics, the viscosity of free water is greatly improved for the pores and cracks with small scale²⁸. The viscosity of water applies a reverse force on the development of pores and cracks, which hinders the development of pores and cracks. With the increase of strain rate, the damage and deformation of GC is accelerated, and the ability of free water in pores and cracks to limit its deformation is relatively weakened. Therefore, the extent of the decrease of dynamic peak strain of GC declines with the increase of strain rate.

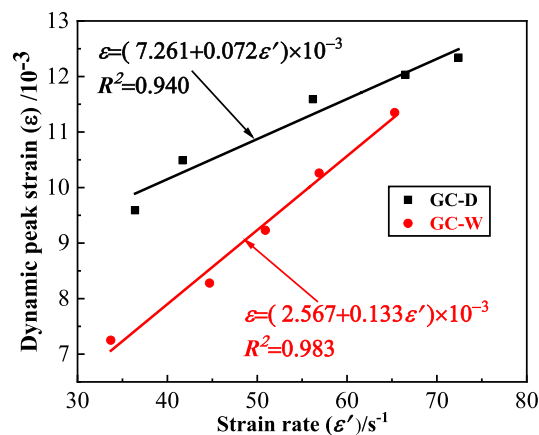


Figure 8. The dynamic peak strain of GC.

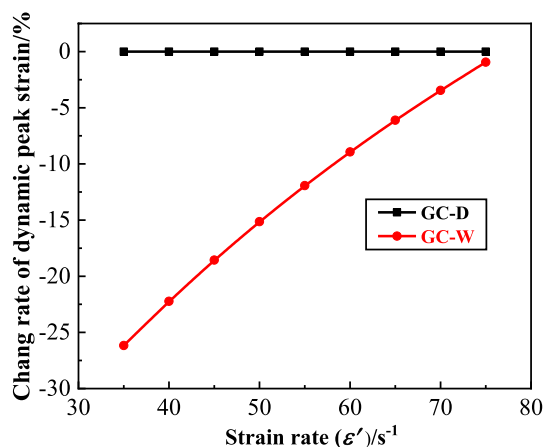


Figure 9. The change rate of dynamic peak strain of GC.

Specific energy absorption

The specific energy absorption (SEA) of GC is shown in Fig. 10. From this figure, with the increase of strain rate, the SEA of GC before or after water saturation gradually increases. At the same strain rate, the SEA of GC after water saturation is smaller than that before water saturation. Thus, the energy absorption characteristics of GC decreases after water saturation. In order to quantitatively analyze the influence of water saturation on the SEA of GC, the change rate of specific energy absorption (\overline{SEA}) is defined, as shown in Eq. (3).

$$\overline{SEA} = (SEA_{GC-W} - SEA_{GC-D})/SEA_{GC-D} \quad (3)$$

where SEA_{GC-W} is the SEA of GC after water saturation, SEA_{GC-D} is the SEA of GC before water saturation. The \overline{SEA} of GC is shown in Fig. 11. From this figure, the \overline{SEA} of GC after water saturation is less than 0, and the minimum is -13.90% . With the increase of strain rate, the \overline{SEA} of GC after water saturation increases. Water saturation can decrease the energy absorption characteristics of GC, but with the increase of strain rate, the extent of the decrease gradually declines.

The decrease of material surface energy due to water saturation is the main factor leading to the decrease of energy absorption characteristics of GC. According to Griffith fracture mechanics theory, the strain energy inside GC gradually increases under loading²⁹. When a limit value is reached, most of the strain energy is released in the form of surface energy, resulting in the formation and expansion of cracks until the specimen is destroyed. Therefore, the formation and development of cracks need to constantly overcome the surface energy of material. According to the Young's equation, the surface energy (γ_{s1}) at the solid–liquid surface can be expressed as Eq. (4)³⁰.

$$\gamma_{s1} = \gamma_s - \gamma_l \cos \theta \quad (4)$$

where γ_s is the surface energy of dry solid, γ_l is the surface energy of saturated liquid, and θ is the contact angle between solid and liquid. From Eq. (4), when the specimen is immersed in water, the water fills the non-closed

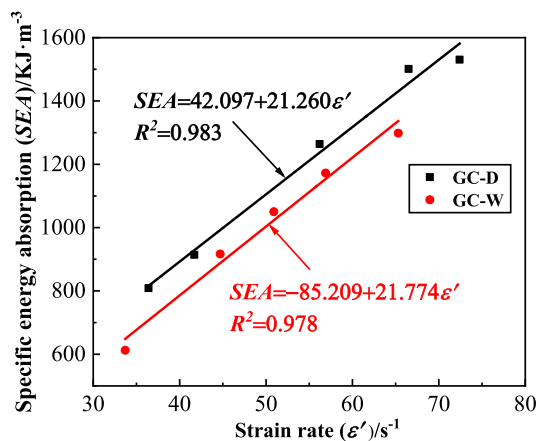


Figure 10. The specific energy absorption of GC.

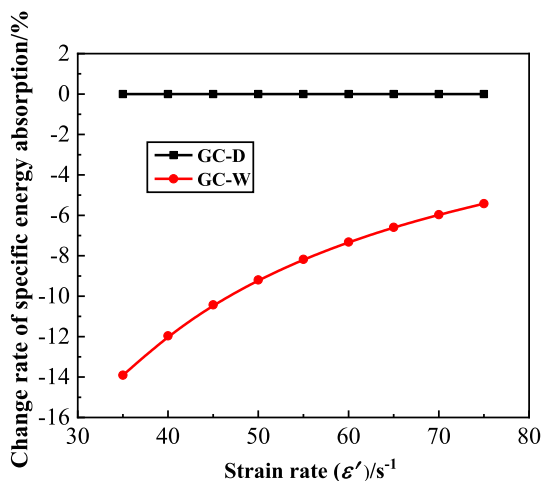


Figure 11. The change rate of specific energy absorption of GC.

pores of the specimen, and the value of θ increases. Because the GC is a hydrophilic material, the value of θ can be approximately taken as 0 after water saturation. So the value of γ_{s1} decreases, that is, the surface energy at the solid–liquid surface decreases. Therefore, the surface energy of the GC needed to overcome after water saturation decreases, which leads to the decrease of the energy absorption characteristics of GC after water saturation. With the increase of strain rate, the accumulation rate of strain energy and development rate of cracks increase, resulting in a relatively small change of the surface energy at the solid–liquid surface. Therefore, the extent of the decrease of energy absorption characteristics of GC after water saturation declines with the increase of strain rate.

Fractal characteristics of fragments

The fragmental morphology and fragment size of the specimen can directly reflect the damage degree of GC. The impact fragmental morphology of GC is shown in Fig. 12. From this figure, it is difficult to judge the damage degree and internal damage of the specimen. Fractal dimension is an important concept in fractal theory to characterize the complexity and irregularity of fractal sets³¹. Due to the complexity and disorder of damage of GC under impact load, it is a typical nonlinear problem³². And it is difficult to use traditional theory to quantitatively describe the damage evolution behavior of GC. Therefore, the fractal dimension is used to quantify the damage degree and internal damage of the specimen.

The fragment size of concrete conforms to the G-G-S distribution³³, and the distribution equation is shown in Eq. (5)³⁴.

$$\begin{aligned} y &= M(r)/M_T = (r/r_m)^b \\ N &= r^{-D_b} \end{aligned} \quad (5)$$

where the D_b and M_T are the fractal dimension and the total mass of fragments, respectively. The r and r_m are the size and maximum size of fragments, respectively. the N and $M(r)$ are the number and cumulative mass of fragments with particle size larger than r , respectively.

Because it is difficult to accurately calculate the number of fragments of each particle size, the relationship between the dN and the dM of fragments is considered, as shown in Eq. (6).

$$dM \sim r^3 dN \quad (6)$$

where the dN and dM are the number increment and the mass increment of fragments, respectively.

The Eq. (5) are differentiated and substituted to Eq. (6), then the fractal dimension ($D_b = 3 - b$) can be calculated. The slope of $\ln[M(r)/M_T] - \ln r$ curve is $3 - D_b$. And there is a positive correlation among the damage degree and internal damage of specimen and fractal dimension.

The specimen fragments were sieved by standard sieves, and the mass of the retained fragments on each sieve was weighed, then the $\ln[M(r)/M_T] - \ln r$ curves of GC were drawn, as shown in Fig. 13. From this figure, the data have good linear correlation in the double logarithmic coordinates, indicating that the fragment size distribution has fractal characteristics. The fractal dimension of GC fragments is shown in Fig. 14. From this figure, the fractal dimension of GC fragments before water saturation is 1.780 ~ 2.113, and that after water saturation is 1.635 ~ 1.994. With the increase of strain rate, the fractal dimension of fragments increases. The larger the impact velocity, the greater the degree of damage. And the strain rate is positively correlated with the impact velocity. Therefore, with the increase of strain rate, the damage degree and internal damage of concrete increase, and the fractal dimension of fragments increases. With the same strain rate, the fractal dimension of GC after water

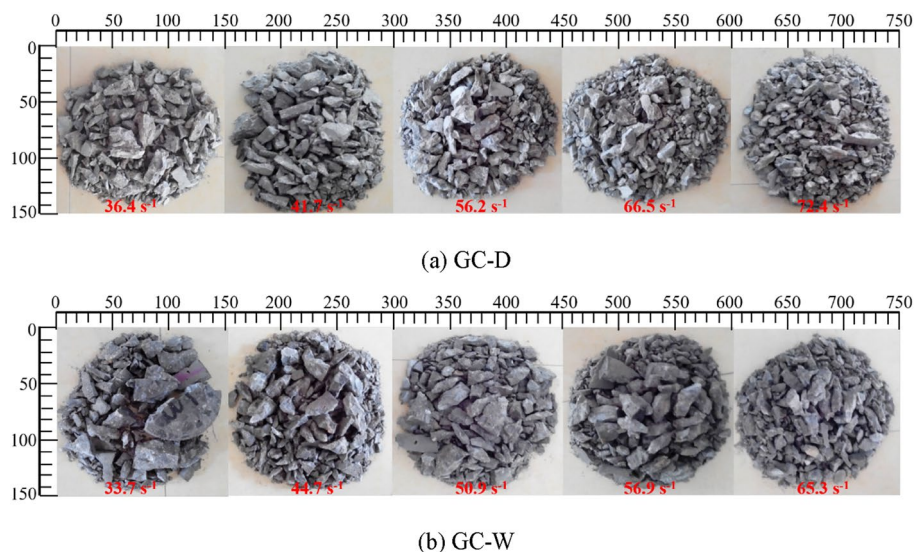


Figure 12. The impact fragmental morphology of GC.

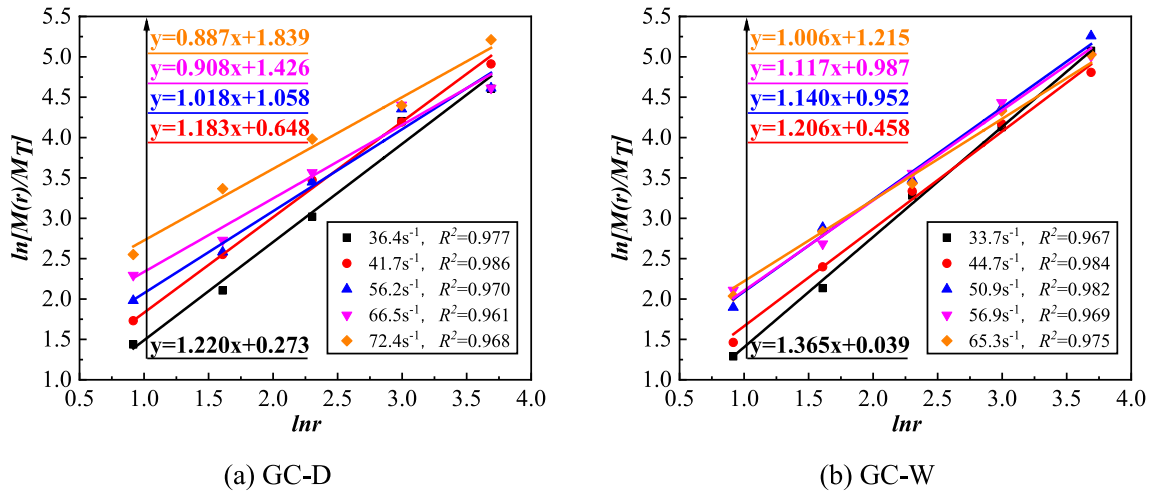


Figure 13. The $\ln[M(r)/M_T]$ - $\ln r$ curves of GC.

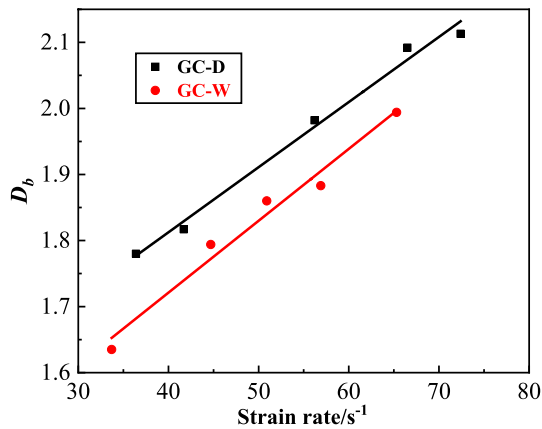


Figure 14. The fractal dimension of GC fragments.

saturation is smaller than that before water saturation, which is due to the viscous resistance effect of free water. The free water reduces the cracking degree of GC after water saturation.

Dynamic constitutive model

Idea of model construction

Firstly, according to Weibull statistical damage distribution theory, a static damage constitutive model for GC is established. Then the static damage constitutive model is modified by introducing strain rate strengthening factor and water saturation influence factor, and the dynamic constitutive model of GC after water saturation is obtained. Finally, the model parameters are calibrated and the accuracy of the model is verified according to the existing test results.

Static damage constitutive model

Based on the statistical damage theory, the static damage constitutive model of GC is established³⁵. The damage variable (D) is defined based on the change of elastic modulus, as shown in Eq. (7).

$$D = 1 - \frac{E_f}{E} \tag{7}$$

where E and E_f are the initial and effective elastic modulus, respectively. And the damage constitutive model of materials can be expressed as Eq. (8) based on the linear damage mechanics theory³⁶.

$$\sigma = E(1 - D)\epsilon \tag{8}$$

It is assumed that GC is composed of a large number of micro-units. On the one hand, these micro-units are large enough to contain many damage defects. On the other hand, these micro-units are small enough to be treated as particles compared to the whole concrete structure. Because the distribution of damage defects in concrete is random, it can be considered that the strength distribution of these micro-elements is random.

The existing researches have shown that the randomness of the micro-unit strength distribution of the above materials can usually be characterized by some statistical laws, such as Weibull distribution, normal distribution, power function distribution, etc.^{37,38}. And for concrete, its strength distribution of micro-units usually conforms to Weibull distribution³⁹.

Therefore, in order to combine the damage theory and statistical theory to construct the corresponding statistical damage constitutive model, this study makes the following assumptions.

- (1) The strength distribution of micro-units of GC follows two-parameter Weibull distribution, and its probability density distribution function is Eq. (9).

$$P(F) = \frac{m}{F_0} \left(\frac{F}{F_0} \right)^{m-1} e^{-\left(\frac{F}{F_0} \right)^m} \quad (9)$$

where F is the strength variable of micro-units, m and F_0 are Weibull distribution parameters.

- (2) The damage evolution of geopolymetric concrete under loading can be regarded as a continuous process of micro-units cumulative failure. The decrease of the elastic modulus of GC at damaged state can be expressed as the failure of a certain number of micro-units. So the damage variable (D) can be expressed as Eq. (10).

$$D = N_f / N \quad (10)$$

where the N and N_f are the number of all micro-units and destroyed micro-units.

Based on the above assumption, when the load increases from 0 to F , the N_f is shown in Eq. (11).

$$N_f = \int_0^F NP(F)dF = N \left(1 - e^{-\left(\frac{F}{F_0} \right)^m} \right) \quad (11)$$

Equation (10) is substituted to Eqs. (11), and (12) is obtained.

$$D = 1 - e^{-\left(\frac{F}{F_0} \right)^m} \quad (12)$$

Equation (12) is substituted to Eq. (8), and the static damage constitutive model of GC can be obtained, as shown in Eq. (13).

$$\sigma = E\varepsilon e^{-\left(\frac{F}{F_0} \right)^m} \quad (13)$$

The strength (F) of micro-units in this model has different expressions under different strength criterion. Based on the Mohr–Coulomb strength criterion, F can be expressed as Eq. (14)⁴⁰.

$$F = E\varepsilon(1 + \sin \varphi) \quad (14)$$

where the φ is the internal friction angle.

Dynamic constitutive model

Modification of static damage constitutive model

Strain rate and water saturation have significant effects on the stress (σ) of GC. Therefore, the static damage constitutive model is modified by introducing strain rate strengthening factor and water saturation influence factor.

- (1) Strain rate strengthening factor

The strain rate strengthening factor (R_{sr}) is introduced on the basis of Eq. (13), as shown in Eq. (15).

$$\sigma = R_{sr} E\varepsilon e^{-\left(\frac{F}{F_0} \right)^m} \quad (15)$$

In the existing researches, R_{sr} is usually defined as an increasing function of strain rate to reflect the strengthening effect of strain rate. For example, in the HJC constitutive model, the strain rate strengthening factor is defined as $R_{sr} = 1 + C_0 \ln \varepsilon'^*$, where C_0 is the strain rate coefficient and ε'^* is the dimensionless strain rate. In this study, R_{sr} is defined as Eq. (16).

$$R_{sr} = B_1 + B_2 \log(\varepsilon') + B_3 [\log(\varepsilon')]^2 \quad (16)$$

where ε' is strain rate, B_1 , B_2 and B_3 are model parameters.

- (2) Water saturation influence factor.

On the basis of introducing the strain rate strengthening factor, the water influence factor (R_w) is further introduced, as shown in Eq. (17).

$$\sigma = R_{sr} R_w E\varepsilon e^{-\left(\frac{F}{F_0} \right)^m} \quad (17)$$

R_w is defined as a function of the strain rate (ε'), as shown in Eq. (18).

$$R_w = B_4 + B_5 \log(\varepsilon') \quad (18)$$

where B_4 and B_5 are model parameters.

In addition, in the process of calibrating the model parameters, it is found that the distribution parameters (m , F_0) have great influence on the shape of the stress–strain curve, and their values are different at different strain rates. Therefore, in order to improve the accuracy of the model and facilitate parameters fitting, the distribution parameters (m , F_0) are defined as functions of the strain rate (ε'), respectively, as shown in Eq. (19).

$$\begin{cases} m = H_1 + H_2 \log(\varepsilon') + H_3 [\log(\varepsilon')]^2 \\ F_0 = H_4 + H_5 \log(\varepsilon') + H_6 [\log(\varepsilon')]^2 \end{cases} \quad (19)$$

where $H_1 \sim H_6$ are model parameters.

Finally, through the corresponding modification, the dynamic constitutive model of GC after water saturation can be obtained, as shown in Eq. (20).

$$\sigma = \left\{ B_1 + B_2 \log(\varepsilon') + B_3 [\log(\varepsilon')]^2 \right\} [B_4 + B_5 \log(\varepsilon')] E \varepsilon e^{-\left(\frac{F}{F_0}\right)^m} \quad (20)$$

where $F = E\varepsilon(1 + \sin \varphi)$.

Parameters calibration

According to Eq. (19), the dynamic constitutive model of GC after water saturation contains the following parameters, $B_1 \sim B_5$, $H_1 \sim H_6$, E and φ . The specific determination method of them is as follows.

- (1) The secant modulus is taken as elastic modulus (E), namely $E = (\sigma_{0.6} - \sigma_{0.4}) / (\varepsilon_{0.6} - \varepsilon_{0.4})$. Where, $\sigma_{0.6} = 0.6f$, $\sigma_{0.4} = 0.4f$, and f is the peak stress. $\varepsilon_{0.6}$ and $\varepsilon_{0.4}$ are the corresponding strains when the stress is $\sigma_{0.6}$ and $\sigma_{0.4}$ on the rising section of the stress–strain curve, respectively.
- (2) According to the peak stress of GC-D and GC-W in Fig. 8, the values of $B_1 \sim B_5$ can be obtained by regression analysis. The values of $B_1 \sim B_5$ after regression analysis are shown in Table 2. It should be noted that when Eq. (20) is used for GC-D, B_4 is 1 and B_5 is 0, that is, R_w is 1.
- (3) m and F_0 are repeatedly calibrated according to the experimental stress–strain curves, and then the values of $H_1 \sim H_6$ are obtained by regression analysis, as shown in Table 3.
- (4) φ is obtained by further adjusting and calibrating according to the experimental stress–strain curves based on the existing empirical value³¹. According to the research results in Reference³⁵, the value of φ has little effect on the fitting results of the model, so this parameter determination method will not have a great influence on the accuracy of the model.

Model verification

In order to verify the accuracy of the model, the model fitting curves and experimental stress–strain curves of GC-D and GC-W are shown in Fig. 15. From this figure, in general, the model fitting curves is in good agreement with the experimental stress–strain curves, and the characteristic strength and strain are close to each other, which shows that the modeling method adopted in this study is feasible and the dynamic constitutive model can accurately reflect the impact mechanical behavior of GC after water saturation. The dynamic constitutive model in this study has certain engineering practical value for the design calculation, stress analysis and safety evaluation of underwater GC structure. Meanwhile, it can also provide some reference for the corresponding numerical simulation.

B1	B2	B3	B4	B5
−5.225	7.212	−1.898	0.784	0.164

Table 2. The values of $B_1 \sim B_5$.

	H1	H2	H3	H4	H5	H6
GC-D	−124.445	149.225	−42.489	0.009	0.007	−0.002
GC-W	−330.360	412.119	−125.834	0.163	−0.192	0.061

Table 3. The values of $H_1 \sim H_6$.

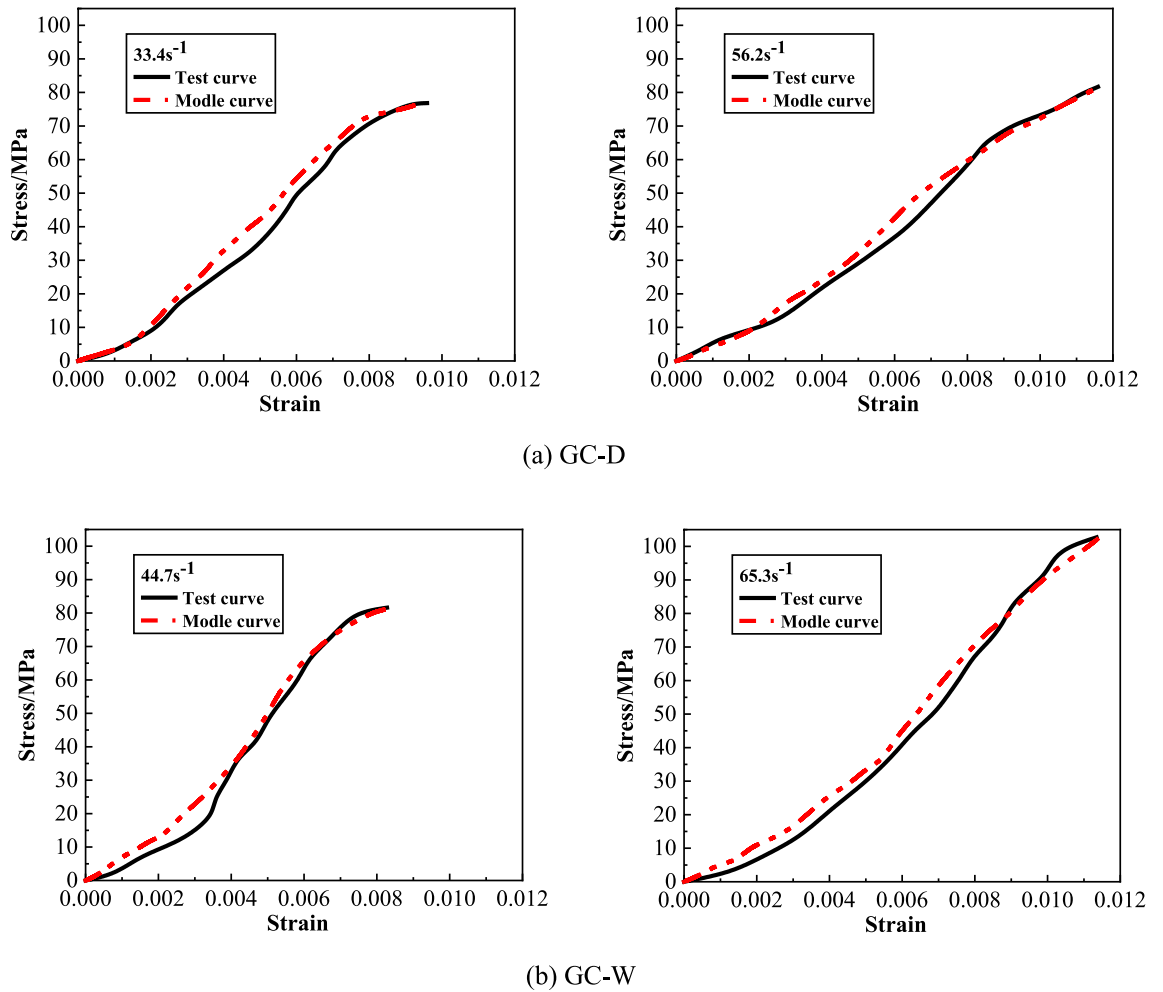


Figure 15. Comparison between model fitting curves and experimental curves.

Conclusion

The dynamic compressive test of geopolymer concrete (GC) before and after water saturation was carried out, and the effects of water saturation and strain rate on the impact toughness and fracture morphology of GC were studied. Based on Weibull statistical damage distribution theory, the dynamic constitutive model of GC after water saturation was constructed. The main conclusions are as follows.

- (1) The dynamic peak strain and specific energy absorption of GC before or after water saturation have strain rate strengthening effect. The impact toughness of GC decreases after water saturation.
- (2) The dynamic peak strain and specific energy absorption of GC decrease after water saturation, and the maximum extent of the decrease are 26.16 and 13.90%, respectively.
- (3) The size distribution of GC fragments before or after water saturation has fractal characteristics. The fractal dimension of GC fragments after water saturation is smaller than that before water saturation.
- (4) The modeling method based on Weibull statistical damage distribution theory is feasible. The dynamic constitutive model fitting curves are in good agreement with the experimental stress–strain curves.

Data availability

The data that support the findings of this study are available on request from the corresponding author.

Received: 22 August 2023; Accepted: 21 March 2024

Published online: 26 March 2024

References

1. Singh, S., Kant, S. S. & Abdul, A. M. Developing zero carbon emission pavements with geopolymer concrete: A comprehensive review. *Transp. Res. Part D* **110**, 103436 (2022).
2. Danish, A. *et al.* Sustainability benefits and commercialization challenges and strategies of geopolymer concrete: A review. *J. Build. Eng.* **58**, 105005 (2022).

3. Unis, A. H. *et al.* Geopolymer concrete as a cleaner construction material: An overview on materials and structural performances. *Cleaner Mater.* **5**, 100111 (2022).
4. Pradhan, P. *et al.* Durability characteristics of geopolymer concrete—Progress and perspectives. *J. Build. Eng.* **59**, 105100 (2022).
5. Mohammed, A. A., Ahmed, H. U. & Mosavi, A. Survey of mechanical properties of geopolymer concrete: A comprehensive review and data analysis. *Materials* **14**(16), 4690 (2021).
6. Amran, M. *et al.* Long-term durability properties of geopolymer concrete: An in-depth review. *Case Stud. Constr. Mater.* **15**, e00661 (2021).
7. Zhang, G. H., Li, X. H. & Li, Z. L. Experimental study on static mechanical properties and moisture contents of concrete under water environment. *Sustainability* **11**(10), 2962 (2019).
8. Zheng, Z. Q. *et al.* A creep model coupling moisture and mechanical damage for water-bearing concrete. *Constr. Build. Mater.* **326**, 126598 (2022).
9. Xue, L., Cai, R. & Guo, X. Mechanical and frost resistance properties of high air content hydraulic concrete. *Mater. Res. Innov.* **19**(5), 510–513 (2015).
10. Ahmad, Z. F. H. *et al.* Geopolymer as underwater concreting material: A review. *Constr. Build. Mater.* **291**, 123276 (2021).
11. Huang, Y. Y. *et al.* Tensile creep tests of hydraulic concrete under different curing conditions. *J. Mater. Civ. Eng.* **32**(4), 05020004 (2020).
12. Rossi, P. *et al.* The dynamic behaviour of concrete: Influence of free water. *Mater. Struct.* **25**(9), 509–514 (2012).
13. Rossi, P. Influence of cracking in the presence of free water on the mechanical behaviour of concrete. *Mag. Concr. Res.* **43**(154), 53–57 (1991).
14. Metha P K, Nontei P J M. Concrete: Microstructure, properties and materials. Indian Concrete Institute (1997).
15. Vu, X. H. *et al.* Analysis of concrete behaviour under high confinement: Effect of the saturation ratio. *Int. J. Solids Struct.* **46**(5), 1105–1120 (2019).
16. Zhang, Y. L. *et al.* Dynamic mechanical characteristics and mechanism of dry and saturated concrete. *Explos. Shock Waves* **35**(06), 864–870 (2015).
17. Fu, Q. *et al.* Insight into dynamic compressive response of carbon nanotube/carbon fiber-reinforced concrete. *Cement Concr. Compos.* **129**, 104471 (2022).
18. Wang, T. J. *et al.* Coupling effects of axial static pressure ratio and high temperature on dynamic mechanical properties and crushing fractal characteristics of concrete under static-dynamic coupled loads. *J. Build. Eng.* **59**, 105114 (2022).
19. Li, J. H. *et al.* Research on impact toughness and crack propagation of basalt fiber reinforced concrete under SHPB splitting test. *J. Build. Eng.* **77**, 107445 (2023).
20. Geng, K. Q. *et al.* Exploring the brittleness and fractal characteristics of basalt fiber reinforced concrete under impact load based on the principle of energy dissipation. *Mater. Struct.* **55**(2), 78 (2022).
21. Ren, W. B. *et al.* Dynamic mechanical properties of geopolymer concrete after water immersion. *Ceram. Int.* **41**(9), 11852–11860 (2015).
22. Liu, F. D., Xu, J. Y. & Liu, J. L. Mechanical properties of polymer concrete in water site under impact load. *Bull. Chin. Ceram.* **34**(11), 3298–3302 (2015).
23. Zhou, Y. *et al.* Study on the damage behavior and energy dissipation characteristics of basalt fiber concrete using SHPB device. *Constr. Build. Mater.* **368**, 130413 (2023).
24. Geng, K. Q. *et al.* Damage evolution, brittleness and solidification mechanism of cement soil and alkali-activated slag soil. *J. Mater. Res. Technol.* **25**, 6039–6060 (2023).
25. Wang, Z. H. *et al.* Effect of nano-SiO₂ and nano-CaCO₃ on the static and dynamic properties of concrete. *Sci. Rep.* **12**(1), 907 (2022).
26. Guo, H. *et al.* Influence of a hybrid combination of steel and polypropylene fibers on concrete toughness. *Constr. Build. Mater.* **275**, 122132 (2021).
27. Wang, H. L. & Li, Q. B. Micromechanics mechanism of static and dynamic compressive strength variation of saturated concrete. *J. Hydraul. Eng.* **37**(8), 958–962 (2006).
28. Zheng, D. & Li, Q. B. An explanation for rate effect of concrete strength based on fracture toughness including free water viscosity. *Eng. Fract. Mech.* **71**(16), 2319–2327 (2004).
29. Yu, X. Z. *Fracture Mechanics of Rock and Concrete* (Central South University of Technology Press, 1991).
30. Hiromichi, M. & Kouzou, O. Influence of surface energy on compressive strength of concrete under static and dynamic loading. *J. Adv. Concr. Technol.* **4**(3), 409–421 (2006).
31. Yang, X. *et al.* Fractal dimension of concrete meso-structure based on X-ray computed tomography. *Powder Technol.* **350**, 91–99 (2019).
32. Wang, L. *et al.* Effect of fineness and content of phosphorus slag on cement hydration, permeability, pore structure and fractal dimension of concrete. *Fractals* **29**(02), 2140004 (2021).
33. Dong, Y. G., Li, H. J. & Hao, S. W. A study on the relationship between shear fracture energy of concrete and fractal dimension. *J. Exp. Mech.* **18**(4), 466–472 (2003).
34. Cao, M. S. *et al.* Experimental study on fractal characterization in damages of concrete structures. *Rock Soil Mech.* **26**(10), 1570–1574 (2005).
35. Zhu J. J. Experimental study on mechanical properties and damage model of rock under cyclic impact load. Changsha: Central South University (2012).
36. Lemaitre, J. *A Course on Damage Mechanics* (Springer, 1992).
37. Ning, J. G., Shang, L. & Sun, Y. X. Empirical formula, strength theory and phenomenological constitutive model of concrete material dynamic behavior. *Adv. Mech.* **36**(3), 389–405 (2006).
38. Li, S. C. *et al.* Study on rock damage constitutive model based on Weibull distribution. *J. Hunan Univ. Sci. Technol. Nat. Sci. Edn.* **22**(4), 65–68 (2008).
39. Long, Y. *et al.* Damage evolution analysis of steel fiber reinforced concrete materials based on Weibull probability distribution. *J. Mater. Sci. Eng.* **25**(6), 830–832 (2008).
40. Chen, X., Wu, S. & Zhou, J. Experimental study and analytical formulation of mechanical behavior of concrete. *Constr. Build. Mater.* **47**, 662–670 (2013).

Acknowledgements

The authors would like to appreciate the financial help of the Qingyang City Science and Technology Talent Special Plan Project (Grant no. QY-STK-2022A-002) and University Teacher Innovation Fund Project of 2023 (Grant no. 2023A-145).

Author contributions

Conceptualization, T.Y. and X.Y.; methodology, X.Z. and X.Y.; validation, T.Y.; formal analysis, T.Y.; investigation, X.Z. and X.Y.; resources, X.Z.; data curation, T.Y.; writing—original draft preparation, T.Y. and X.Y.; writing—review

and editing, T.Y., X.Y. and X.Z.; visualization, X.Z.; supervision, T.Y.; project administration, T.Y.; funding acquisition, T.Y. and X.Z..

Competing interests

The authors declare no competing interests.

Additional information

Correspondence and requests for materials should be addressed to X.Y.

Reprints and permissions information is available at www.nature.com/reprints.

Publisher's note Springer Nature remains neutral with regard to jurisdictional claims in published maps and institutional affiliations.



Open Access This article is licensed under a Creative Commons Attribution 4.0 International License, which permits use, sharing, adaptation, distribution and reproduction in any medium or format, as long as you give appropriate credit to the original author(s) and the source, provide a link to the Creative Commons licence, and indicate if changes were made. The images or other third party material in this article are included in the article's Creative Commons licence, unless indicated otherwise in a credit line to the material. If material is not included in the article's Creative Commons licence and your intended use is not permitted by statutory regulation or exceeds the permitted use, you will need to obtain permission directly from the copyright holder. To view a copy of this licence, visit <http://creativecommons.org/licenses/by/4.0/>.

© The Author(s) 2024